International Journal of Minerals, Metallurgy and Materials
Volume 21, Number 11, November 2014, Page 1068
DOI: 10.1007/s12613-014-1011-9

Formation mechanism and control of $MgO·Al_2O_3$ inclusions in non-oriented silicon steel

Yan-hui Sun, Ya-nan Zeng, Rui Xu, and Kai-ke Cai

School of Metallurgical and Ecological Engineering, University of Science and Technology Beijing, Beijing 100083, China
(Received: 20 February 2014; revised: 22 June 2014; accepted: 23 June 2014)

Abstract: On the basis of the practical production of non-oriented silicon steel, the formation of $MgO·Al_2O_3$ inclusions was analyzed in the process of "basic oxygen furnace (BOF) → RH → compact strip production (CSP)". The thermodynamic and kinetic conditions of the formation of $MgO·Al_2O_3$ inclusions were discussed, and the behavior of slag entrapment in molten steel during RH refining was simulated by computational fluid dynamics (CFD) software. The results showed that the MgO/Al_2O_3 mass ratio was in the range from 0.005 to 0.017 and that $MgO·Al_2O_3$ inclusions were not observed before the RH refining process. In contrast, the MgO/Al_2O_3 mass ratio was in the range from 0.30 to 0.50, and the percentage of $MgO·Al_2O_3$ spinel inclusions reached 58.4% of the total inclusions after the RH refining process. The compositions of the slag were similar to those of the inclusions; furthermore, the critical velocity of slag entrapment was calculated to be 0.45 $m·s^{-1}$ at an argon flow rate of 698 $L·min^{-1}$, as simulated using CFD software. When the test steel was in equilibrium with the slag, [Mg] was 0.00024wt%–0.00028wt% and $[Al]_s$ was 0.31wt%–0.37wt%; these concentrations were theoretically calculated to fall within the $MgO·Al_2O_3$ formation zone, thereby leading to the formation of $MgO·Al_2O_3$ inclusions in the steel. Thus, the formation of $MgO·Al_2O_3$ inclusions would be inhibited by reducing the quantity of slag entrapment, controlling the roughing slag during casting, and controlling the composition of the slag and the MgO content in the ladle refractory.

Keywords: silicon steel; steelmaking; inclusions; deoxidation; slag entrapment; thermodynamics; kinetics

1. Introduction

As the demand for high-quality iron and steel products increases, the demand for non-oriented electrical steels will continue to grow in the coming years. Non-oriented silicon steel with ultra-low carbon and high silicon and aluminum contents should be rolled into silicon steel sheet via hot rolling and cold rolling processes. However, surface defects and other problems inhibit its production. The defects may be affected by $MgO·Al_2O_3$ spinel inclusions formed during aluminum deoxidation. Theoretically, the MgO/Al_2O_3 mass ratio should be 0.392 in pure spinel inclusions. However, the MgO contents in inclusions range from 6.5wt% to 39.0wt%, and this compound exhibits properties similar to those of $MgO·Al_2O_3$ spinel inclusions. $MgO·Al_2O_3$ spinel inclusions exist as C-type inclusions, with a small aspect ratio. This type of inclusion causes surface defects and other problems, especially line defects, which are affected by $MgO·Al_2O_3$ inclusions because $MgAl_2O_4$ spinel has a high melting point and exhibits a deformation capacity that differs from that of steel. In addition, spinel inclusions tend to accumulate at the inner walls of submerged entry nozzles, inducing clogging during continuous casting [1–3]. Although these mechanisms can explain the evolution process to a certain extent, some points remain unresolved.

Numerous scholars have published research related to the formation and evolution mechanism of these inclusions [4–11]. In one commonly proposed mechanism, the dissolved Mg and Ca are supplied from the slag and refractory, and the $MgO–Al_2O_3$ system inclusions form by the reaction between alumina inclusions and dissolved Mg. In addition, Kang *et al.* [7] and Jiang *et al.* [10] have indicated that the $MgO–Al_2O_3$ system is not stable when present in trace

Corresponding author: Yan-hui Sun E-mail: sun_yanhui@163.com

quantities.

First, most of these previous studies were conducted in laboratories, where the conditions differ from those used in actual secondary refining processes. For example, the steel of industrial products was commonly used as a raw material; this steel may already contain Mg and Ca, and its Mg and Ca contents therefore differ from those of steels used in real refining processes [10–11], where the Mg and Ca contents are often considered to be zero because of the high content of dissolved oxygen after BOF blowing. Consequently, investigating the process by which dissolved Ca and Mg form is difficult in a laboratory setting. Moreover, the laboratory experiments did not include argon stirring, which leads to the enrichment of certain elements in parts of the steel and results in the formation of inclusions, such as MgO inclusions, that rarely form in actual practice. In these previous studies, the $MgO–Al_2O_3$ system inclusions formed prior to $CaO–Al_2O_3$ system inclusions, which was usually attributed to the activity of Mg being higher than that of Ca [7,11]. Without consideration of the process by which dissolved Ca and Mg form, this phenomenon could not be well explained because of dissolved Ca already coexisted with Mg in liquid steel used in these studies [10–11], which is problematic because $MgO–Al_2O_3$ system inclusions are unstable under such conditions. Meanwhile, different views about the process by which the $MgO–Al_2O_3$ system evolves into the $CaO–MgO–Al_2O_3$ system have been reported. Some authors have claimed that Ca substitutes for Al in $MgO–Al_2O_3$ system inclusions during the evolution process [12], whereas most scholars have reported that Mg in the $MgO–Al_2O_3$ system inclusions was substituted.

In the present research, the process by which ordinary inclusions are transformed into compound inclusions consisting of $MgO·Al_2O_3$ and $CaO–Al_2O_3–MgO$ was investigated under practical production conditions. Therefore, our results should provide technical guidance for the development of measures to control the formation of $MgO·Al_2O_3$ inclusions during smelting processes.

2. Experimental

2.1. Smelting process

The industrial experiments were conducted using non-oriented silicon steel, and the steel whose chemical composition is listed in Table 1 was produced by the process of "basic oxygen furnace (BOF) → RH → compact strip production (CSP)". During the tapping of BOF, aluminum and silicomanganese were added to the ladle for composition adjustment. During RH refining, aluminum was used for deoxidation, and the silicomanganese alloy was used to adjust the composition of the non-oriented silicon steel. Argon was used at a flow rate of 1300–1500 L/min for agitation during the RH refining process.

Table 1. Chemical composition of non-oriental silicon steel

wt%

C	Si	Mn	P	S
0.001–0.003	1.5–1.7	0.1–0.2	0.03–0.05	0.002–0.003

2.2. Sampling and analysis method

The industrial trials were conducted during five heats using a 70 mm × 1300 mm thin plate. In the experimental procedure, five liquid steel samples were collected using barrel-type samplers; specifically, the samples were collected after Al was added, after silicomanganese was added, when RH refining was complete, from the tundish, and from the slab. For the purpose of investigation, the compositions of the inclusions were analyzed using metallographic microscopy and a scanning electron microscopy in conjunction with energy-dispersive X-ray spectroscopy (SEM-EDS). The RH refining was simulated using computational fluid dynamics (CFD) software.

3. Results and discussion

3.1. Types of inclusions

Typical types of the detected inclusions are listed in Fig. 1. The compositions of the inclusions are showed in Table 2. As evident in the figure, a total of three categories of inclusions were observed: $MgO·Al_2O_3$ system inclusions, $Al_2O_3·SiO_2·MnO·MgO$ system inclusions, and $Al_2O_3·SiO_2·MnO·MnS$ inclusions. All the detected inclusions were small in size, mainly varying in the range of 1–2 μm, as shown in Fig. 1.

3.2. Evolution of inclusion types during each process

A total of 111, 203, 114, and 160 inclusions in samples collected after Al was added during the RH refining process, after the silicomanganese was added during the RH refining process, from the tundish, and from the slab, respectively, were analyzed by metallographic microscopy. The compositions of the inclusions were analyzed by SEM-EDS; the results are plotted in $Al_2O_3–SiO_2–MgO$ ternary phase diagrams in Fig. 2.

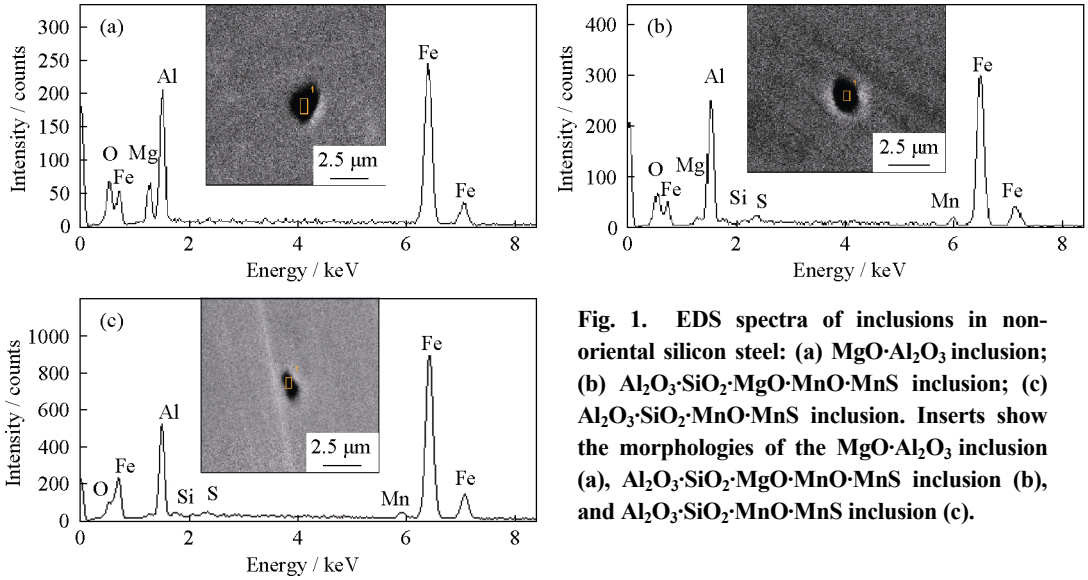

Fig. 1. EDS spectra of inclusions in non-oriental silicon steel: (a) $MgO{\cdot}Al_2O_3$ inclusion; (b) $Al_2O_3{\cdot}SiO_2{\cdot}MgO{\cdot}MnO{\cdot}MnS$ inclusion; (c) $Al_2O_3{\cdot}SiO_2{\cdot}MnO{\cdot}MnS$ inclusion. Inserts show the morphologies of the $MgO{\cdot}Al_2O_3$ inclusion (a), $Al_2O_3{\cdot}SiO_2{\cdot}MgO{\cdot}MnO{\cdot}MnS$ inclusion (b), and $Al_2O_3{\cdot}SiO_2{\cdot}MnO{\cdot}MnS$ inclusion (c).

Table 2. Chemical composition of inclusions in Fig. 1 at%

Fig. 1	Mg	Al	O	Mn	S	Si	Fe
(a)	8.12	23.01	31.90	—	—	—	36.98
(b)	1.35	25.85	26.83	2.17	1.29	0.82	41.68
(c)	—	25.35	10.85	1.50	1.32	0.84	60.14

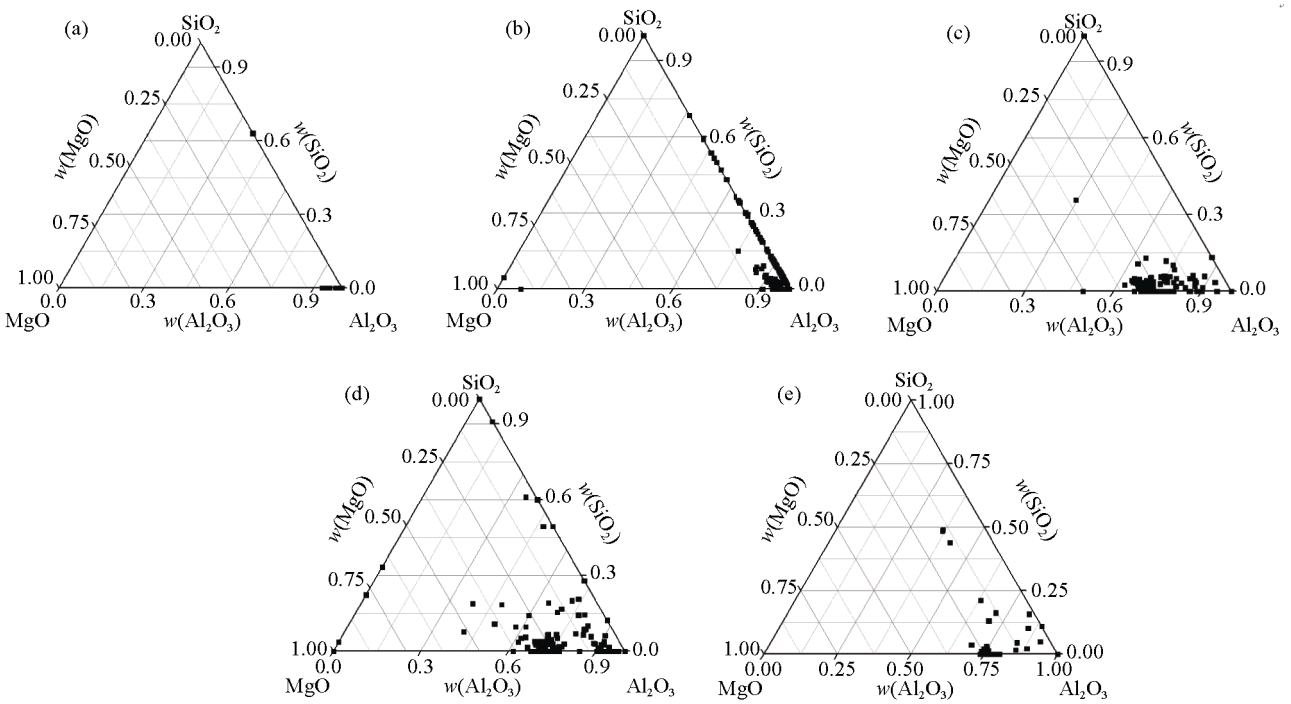

Fig. 2. Ternary phase diagrams of Al_2O_3–SiO_2–MgO inclusions during the smelting process: (a) after the addition of Al; (b) after the addition of silicomanganese; (c) from the tundish; (d) from the slab; (e) compositions of adhesion on the inner face of the submerged nozzle.

Typical Al_2O_3 inclusions were mainly observed in the sample collected after Al was added during the RH refining process, as shown in Fig. 2(a). After silicomanganese was added to molten steel, $Al_2O_3{\cdot}SiO_2$ inclusions were observed in the samples, as presented in Fig. 2(b). Furthermore, after the RH refining process, the $Al_2O_3{\cdot}SiO_2$ inclusions started to

transform into $MgO·Al_2O_3$ and $CaO–Al_2O_3–MgO$ system inclusions, which were observed in the sample collected from the tundish, as depicted in Fig. 2(c). Moreover, the $CaO–Al_2O_3–MgO$ inclusions in the tundish sample mostly transformed into $Al_2O_3·SiO_2·MgO$ inclusions in the slab samples, as shown in Fig. 2(d). In addition, adhesion on the inner face of the submerged nozzle was investigated; interestingly, results in Fig. 2(e) indicate that the 1–9 mm adhesion was predominantly $CaO·6Al_2O_3$ and $MgO·Al_2O_3$ complex inclusions, similar to results observed in the tundish sample. The melting point of $MgO·Al_2O_3$ inclusions was higher than those of other ordinary inclusions; therefore, the submerged nozzle would be blocked by $CaO·6Al_2O_3$ and $MgO·Al_2O_3$ complex inclusions. According to the aforementioned results, the ordinary inclusions gradually changed into $MgO·Al_2O_3$ inclusions after silicomanganese was added during the RH refining process. Therefore, elucidation of the formation mechanism of $MgO·Al_2O_3$ inclusions in the RH refining process could solve the surface-quality and castability problems associated with non-oriented silicon steel.

3.3. Distribution of MgO inclusions in each process

The MgO contents of inclusions in samples collected during various stages of the RH refining and continuous casting process were analyzed by SEM-EDS. The variations in MgO content of the inclusions are shown in Fig. 3 for samples collected after Al was added, after silicomanganese was added, when the RH refining was complete, from the tundish, and from the slab, respectively. The MgO contents of inclusions in samples collected after Al deoxidation and silicomanganese addition processes were 17.9wt% and 18.1wt%, respectively. The MgO contents of inclusions in samples collected after RH refining, from the tundish, and from the slab were 96.0wt%, 96.4wt%, and 88.4wt%, respectively.

3.4. Changes in MgO/Al_2O_3 ratio during each process

For all of the steel samples, the MgO and Al_2O_3 contents of inclusions in samples collected after Al was added, after silicomanganese was added, after RH refining was complete, from the tundish, and from the slab, were analyzed by SEM-EDS. In this study, $MgO·Al_2O_3$ was defined as the value of MgO/Al_2O_3 in the range from 0.3 to 0.5. The statistical results for the MgO/Al_2O_3 mass ratios in the inclusions are presented in Fig. 4.

The MgO/Al_2O_3 mass ratios of inclusions were only 0.005 and 0.017 in samples collected after Al was added and after silicomanganese was added. In contrast, the corresponding ratios of inclusions in samples collected after RH refining was complete, from the tundish, and from the slab samples increased to 0.378, 0.316, and 0.285, respectively. These results indicate that interaction among liquid steel, ladle lining, and refractory material at the RH submerged tube and in the top slag occurred during the RH refining process. Therefore, $MgO·Al_2O_3$ inclusions started to form after RH refining, as presented in Fig. 4. Furthermore, the compositions of the top slag were analyzed by X-ray diffraction (XRD). The MgO/Al_2O_3 mass ratio in the top slag was in the range of 0.17 to 0.20, which is similar to the compositions of the inclusions. The phenomenon can be explained by slag being entrapped during the RH refining process.

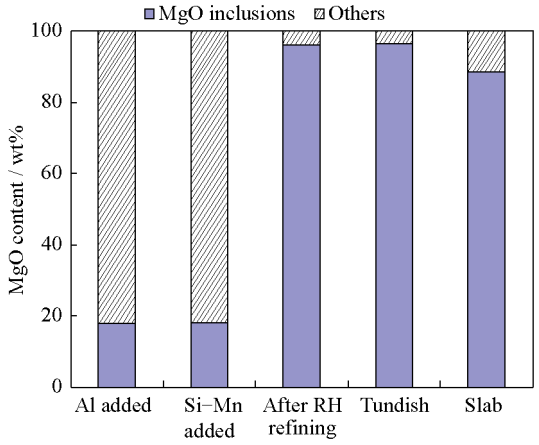

Fig. 3. MgO content of inclusions in samples collected after each process.

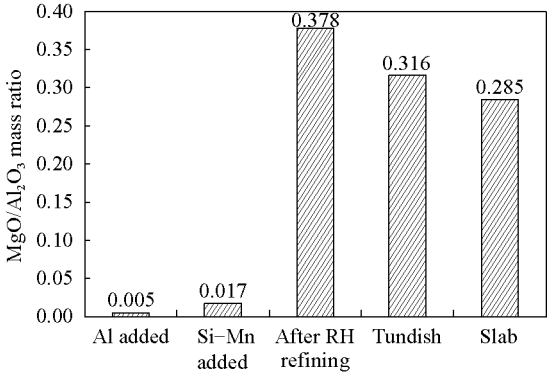

Fig. 4. Average values of MgO/Al_2O_3 mass ratio after each process.

3.5. Distribution of $MgO·Al_2O_3$ spinel inclusions in samples collected after each process

Theoretical research indicated that the inclusions would occur as $MgO·Al_2O_3$ spinel inclusions when the MgO/Al_2O_3 mass ratio reached 0.392. Fig. 5 shows the frequency of occurrence of $MgO·Al_2O_3$ spinel inclusions in samples col-

lected after each process. Almost no $MgO{\cdot}Al_2O_3$ inclusions were present in samples collected after Al was added and after silicomanganese was added. However, the percentage of $MgO{\cdot}Al_2O_3$ spinel inclusions reached 58.4% of the total inclusions in the sample collected after RH refining; the percentages of other inclusions, such as $MgO{\cdot}Al_2O_3{\cdot}SiO_2$, $MgO{\cdot}Al_2O_3{\cdot}SiO_2{\cdot}MnS$, and $MgO{\cdot}Al_2O_3{\cdot}CaO$, was 41.6wt%. The percentage of $MgO{\cdot}Al_2O_3$ spinel inclusions in the sample collected from the tundish was 59.0wt%, which was almost equal to that in the sample collected after RH refining. The percentage of $MgO{\cdot}Al_2O_3$ spinel inclusions decreased to 46.0wt% in the slab samples. These results can be explained by part of inclusions being removed during the continuous casting process, as shown in Fig. 5.

3.6. Thermodynamic calculations related to the formation of $MgO{\cdot}Al_2O_3$ inclusions

Our results indicated that the formation of $MgO{\cdot}Al_2O_3$ spinel inclusions were possibly affected by lining erosion and slag entrapment. However, the main formation mechanism of $MgO{\cdot}Al_2O_3$ spinel inclusions should be interaction among the slag, molten steel, and inclusions. Moreover, Mg in molten steel plays an important bridge role between the slag and inclusions [2,13]. The following two reactions describe the formation of $MgO{\cdot}Al_2O_3$ spinel inclusions:

$$3(MgO)_{slag} + 2[Al] = (Al_2O_3)_{slag} + 3[Mg] \quad (1)$$

$$3(MgO)_{lining} + 2[Al] = (Al_2O_3)_{slag} + 3[Mg] \quad (2)$$

The formation of $MgO{\cdot}Al_2O_3$ spinel inclusions is discussed in two cases. One case is the reaction between Mg and Al_2O_3, as described in the following reaction:

$$4(Al_2O_3) + 3[Mg] = 3MgO{\cdot}Al_2O_3 + 2[Al] \quad (3)$$

The other is the reaction between Al and MgO [14–18]:

$$4(MgO) + 2[Al] = MgO{\cdot}Al_2O_3 + 3[Mg] \quad (4)$$

(1) We considered the following reaction to calculate the $MgO/MgO{\cdot}Al_2O_3$ boundary:

$$4(MgO) + 2[Al] = MgO{\cdot}Al_2O_3 + 3[Mg] \quad (5)$$

$$\lg K_8 = -33.09 + 50880/T \quad (6)$$

$$K_8 = \frac{a^3_{[Mg]}.a_{MgO{\cdot}Al_2O_3}}{a^2_{[Al]}.a^4_{[MgO]}} = \frac{a_{MgO{\cdot}Al_2O_3}.f^3_{Mg}[\%Mg]^3}{a^4_{[MgO]}.f^2_{Al}[\%Al]^2} \quad (7)$$

(2) To calculate the $MgO{\cdot}Al_2O_3/Al_2O_3$ boundary, we considered the following reaction:

$$4(Al_2O_3) + 3[Mg] = 3MgO{\cdot}Al_2O_3 + 2[Al] \quad (8)$$

$$\lg K_{11} = 34.37 - 46950/T \quad (9)$$

$$K_{11} = \frac{a^2_{[Al]}.a^3_{MgO{\cdot}Al_2O_3}}{a^4_{[Al_2O_3]}.a^3_{[Mg]}} = \frac{a^4_{Al_2O_3}.f^3_{Mg}[\%Mg]^3}{a^4_{MgO{\cdot}Al_2O_3}.f^2_{Al}[\%Al]^2} \quad (10)$$

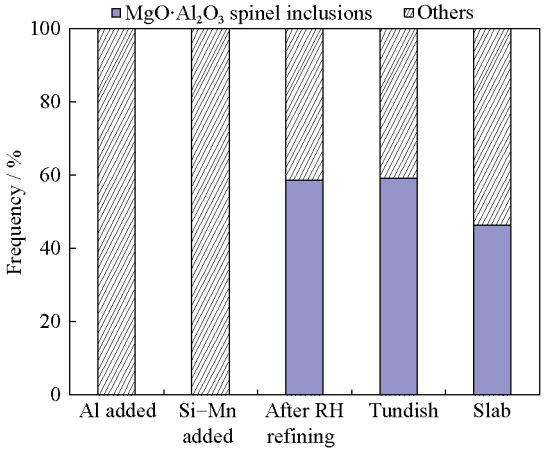

Fig. 5. Frequency of occurrence of $MgO{\cdot}Al_2O_3$ spinel inclusions in each process.

The standard states of oxides are taken as pure solids in Eqs. (7) and (10). By combining Eqs. (6) and (7) and Eqs. (9) and (10) with the interaction coefficients in Table 3, we obtained the chemical compositions and the activities of each oxide in equilibrium and at the boundaries. On the basis of calculations reported by Fujii *et al.* [17], who performed calculations related to the $MgO/MgO{\cdot}Al_2O_3$ boundary at 1873 K, we took the activity of $MgO{\cdot}Al_2O_3$ as 0.8 and that of MgO as 0.99 because of the very poor solubility of Al_2O_3 in MgO. For the $MgO{\cdot}Al_2O_3/Al_2O_3$ boundary, we took the activity of $MgO{\cdot}Al_2O_3$ as 0.47 and that of Al_2O_3 as unity because of the negligibly small solubility of MgO in Al_2O_3. Fig. 6 shows the calculated phase stability diagram of MgO, $MgO{\cdot}Al_2O_3$, and Al_2O_3.

Fig. 6 displays the phase equilibrium diagram of MgO, $MgO{\cdot}Al_2O_3$, and Al_2O_3 at equilibrium between the slag and liquid steel. Al_2O_3 inclusions transformed into $MgO{\cdot}Al_2O_3$ gradually when $[Al]_s$ = 0.0001wt% and $[Mg] \geq 0.806 \times 10^{-6}$wt%. According to our calculation results, $MgO{\cdot}Al_2O_3$ would easily form with increasing Mg and Al content in liquid steel. With increasing Al content, the Mg content required for the formation of $MgO{\cdot}Al_2O_3$ spinel inclusions

Table 3. Interaction coefficients of magnesium and aluminum at 1873 K [2]

Element	C	Si	Mn	P	S	Al_s	Ca	Mg	O	N
Mg	−0.15	−0.09	—	—	−1.38	−0.12	—	0	−430	—
Al	0.091	0.0056	—	0.033	0.030	0.045	0.043	−0.13	−6.6	−0.058

correspondingly increased. When $[Al]_s$ = 0.1wt% and [Mg] $\geq 0.806 \times 10^{-4}$wt%, $MgO{\cdot}Al_2O_3$ started to change into MgO. In practical production processes with the equilibrium between the slag and liquid steel, a large number of $MgO{\cdot}Al_2O_3$ spinel inclusions would form when $[Al]_s$ = 0.32wt% and [Mg] = 0.00025wt%.

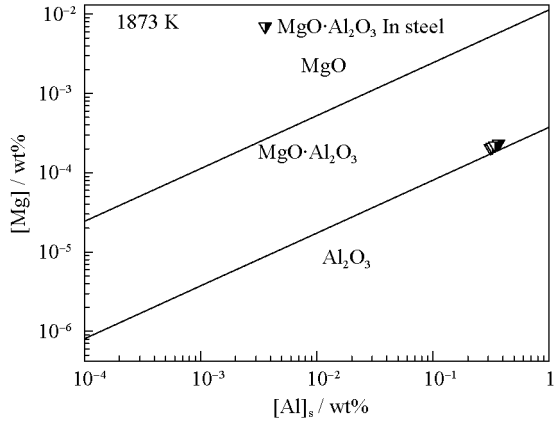

Fig. 6. Phase equilibrium diagram of MgO, $MgO{\cdot}Al_2O_3$, and Al_2O_3.

3.7. Effect of slag entrapment behavior in the RH process on MgO inclusion content

All inclusion types formed during the RH refining process were analyzed by SEM-EDS. The compositions of the top slag were tested by XRD. In addition to pure $MgO{\cdot}Al_2O_3$ spinel inclusions, aluminosilicate inclusions, as $Al_2O_3{\cdot}SiO_2{\cdot}MgO{\cdot}CaO{\cdot}MnS$, were also observed. Fig. 7 displays the variations of MgO/Al_2O_3 mass ratio between the inclusions and the slag. The content of MgO in the top slag was in the range from 5.0wt% to 7.5wt%. As the MgO/Al_2O_3 mass ratio in the slag increased, the MgO/Al_2O_3 mass ratio in the inclusions also increased. These results indicate that the MgO content in the inclusions was affected by the behavior of slag entrapment during the RH refining process.

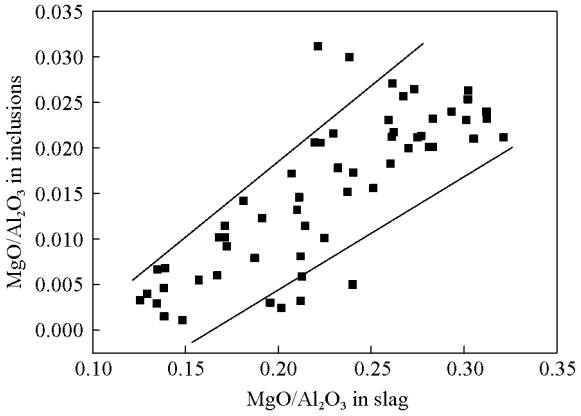

Fig. 7. Effect of MgO/Al_2O_3 mass ratio in the slag on MgO/Al_2O_3 mass ratio in the inclusions.

The EDS and morphological analysis results of typical inclusions in samples after RH refining are presented in Fig. 8. The MgO, Al_2O_3, CaS, and CaO contents were 4.27wt%, 52.49wt%, 1.20wt%, and 42.04wt%, respectively, at point 1 in the inclusion. In contrast, the MgO, Al_2O_3, CaS, and CaO contents were 4.89wt%, 58.24wt%, 2.09wt%, and 34.77wt%, respectively, at point 2. The EDS analysis results also indicated that the compositions of the inclusions were similar to the composition of the top slag. Furthermore, the inclusions were coarser, which indicates that the source of inclusions was slag entrapment during the RH refining process.

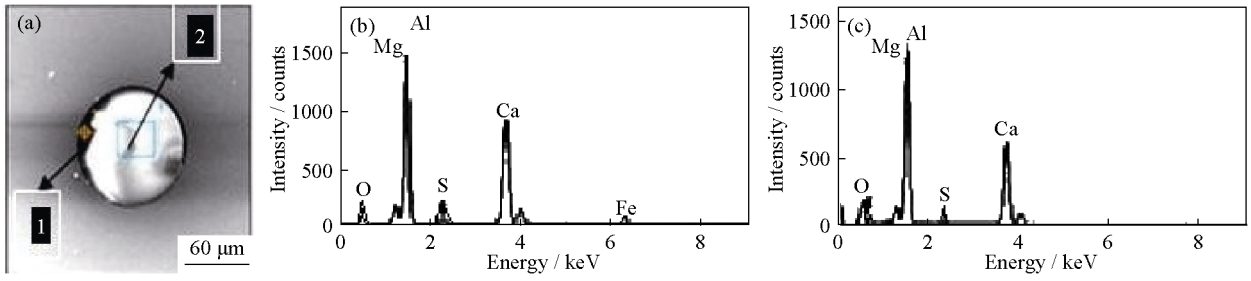

Fig. 8. Typical inclusions in samples collected after the RH refining process (a) and EDS spectra of the inclusion at point 1 (b) and point 2 (c).

3.8. Simulation on slag entrapment during RH refining

To confirm the effect of slag entrapment on inclusion transformation, we used CFD software to simulate the surface velocity of liquid steel in the circulating section under different conditions during the RH refining process. Meanwhile, the critical velocity of slag entrapment ($u_{m,crit}$) was calculated under actual working conditions using the following formula [18]:

$$u_{m,crit} = [128g(\rho_m - \rho_s)\sigma_{ms}\cos\alpha(3\rho_m^2)]^{1/4} \quad (11)$$

where ρ_m is the density of liquid steel, kg/m^3; ρ_s is the density of liquid slag, kg/m^3; σ_{ms} is the interfacial tension of slag/metal, N·m^{-1}; and α is the impact angle of the liquid-steel stream, (°).

Fig. 9 displays velocity contours for Ar flow rates of 920

$L \cdot min^{-1}$ and 1900 $L \cdot min^{-1}$ in the case of liquid steel during the RH refining process. The simulation results indicated that the minimum velocity of liquid steel at the vertical pipe outlet is approximately 0.5 m/s at an Ar flow rate of 920 $L \cdot min^{-1}$. With an increase in Ar flow rate, the velocity of liquid steel at the vertical pipe outlet also increased.

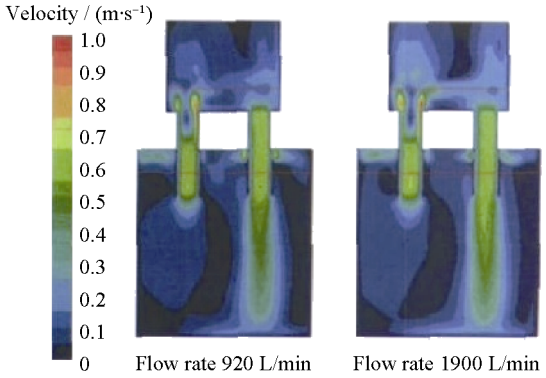

Fig. 9. Velocity contours of liquid steel in RH refining.

A comparison of results for the velocity of slag entrapment between CFD simulation and theoretical calculations is depicted in Fig. 10. The critical velocity of slag entrapment was calculated to be 0.45 $m \cdot s^{-1}$ at an Ar flow rate of 698 $L \cdot min^{-1}$. The simulation results indicate that the surface velocity of liquid steel at an Ar flow rate of 658 $L \cdot m^{-3}$ could not reach 0.45 $m \cdot s^{-1}$, whereas the other surface velocity of liquid steel under different conditions is 0.49–0.57 $m \cdot s^{-1}$, which is greater than the theoretical calculation results. Thus, the results indicate that slag entrapment behavior occurred during the RH refining process.

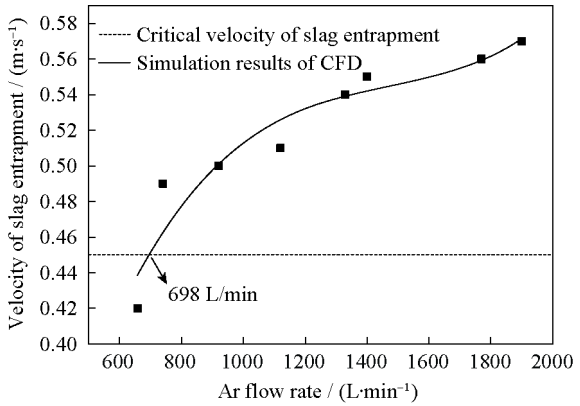

Fig. 10. Relationships between the Ar flowing rate and the velocity of slag entrapment.

3.9. Effect of slag/metal reaction on the formation of $MgO \cdot Al_2O_3$ inclusions

According to our statistical results related to the MgO/Al_2O_3 mass ratio during the RH refining process, as the CaO/Al_2O_3 mass ratio in the slag increases, the MgO/Al_2O_3 mass ratio increases gradually. When the CaO/Al_2O_3 mass ratio is in the range from 2.5 to 3.0 and the MgO/Al_2O_3 mass ratio is in the range from 0.30 to 0.40, $MgO \cdot Al_2O_3$ inclusions begin to form during RH refining, as shown in Fig. 11.

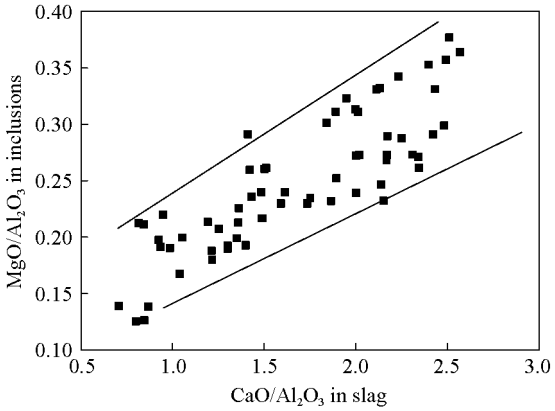

Fig. 11. Effect of CaO/Al_2O_3 mass ratio in the slag on MgO/Al_2O_3 mass ratio in the inclusions.

To explain the effect of the slag on $MgO \cdot Al_2O_3$ inclusions, double films were calculated; the results are presented in Fig. 12. To analyze the reduction reaction of MgO in the slag during the RH refining process, we designed the model to only consider the formation of MgO inclusions, without consideration of other inclusions. From the viewpoint of kinetics, we adopted a competing reaction model based on the two-film theory, which is frequently applied to dephosphorization/desulfurization reactions in molten iron and to reoxidation reactions in molten steel by the slag. In the following discussion, this model will be referred to in abbreviated form as the reaction model [19].

$$[Al] + 1.5[O] = (AlO_{1.5}) \quad (12)$$

$$[Si] + 2[O] = (SiO_2) \quad (13)$$

$$[Mg] + [O] = (MgO) \quad (14)$$

$$K_{Al} = a^*_{AlO_{1.5}} / \left(a^*_{Al} . a^{*1.5}_{O}\right) \quad (15)$$

$$K_{Si} = a^*_{SiO_2} / \left(a^*_{Si} . a^{*2}_{O}\right) \quad (16)$$

$$K_{Mg} = a^*_{MgO} / \left(a^*_{Mg} . a^*_{O}\right) \quad (17)$$

where $a^*_{AlO_{1.5}}$, a^*_{Al}, a^*_{O}, $a^*_{SiO_2}$, a^*_{Si}, a^*_{MgO}, and a^*_{Mg} are the activities of $AlO_{1.5}$, Al, O, SiO_2, Si, MgO, and Mg, respectively. If we assume, on the basis of previous discussion, that the reaction in Eq. (14) is rate-determining for mass transfer on the metal side and that the reaction velocity is expressed considering only mass transfer on the metal side, then Eq. (18) can be deduced using the concentration gradi-

ent in the boundary film on the metal side:

$$\frac{d[Mg]}{dt} = \frac{A}{V} k_m([Mg]^* - [Mg]) \quad (18)$$

where A is the reaction area and k_m is the mass transfer coefficient. This equation reveals that the rate of increase in Mg concentration of molten steel depends on Mg concentration, $[Mg]^*$, at the slag–metal interface. The slag composition dependency of $[Mg]^*$ at the slag–metal interface will be considered qualitatively in the following discussion.

The value of $[Mg]^*$ can be determined by the activity of MgO, a^*_{MgO}, and the activity of oxygen, a^*_O, at the slag–metal interface using Eq. (17). Fig. 12 shows the calculated relationship between the slag basicity, i.e., the CaO/SiO_2 and CaO/Al_2O_3 ratios, and the activity of MgO, a^*_{MgO}, where the latter was obtained using the thermodynamic database software Thermo-calc. The value of a^*_{MgO} increases as the CaO/SiO_2 and CaO/Al_2O_3 ratios of the slag increase. On the basis of the aforementioned results, the $[Mg]^*$ at the slag–metal interface is qualitatively understood to increase at higher slag basicity, as indicated by the CaO/SiO_2 and CaO/Al_2O_3 ratios; consequently, the rate of increase in Mg concentration of molten steel due to the reduction reaction with MgO in the slag also increases.

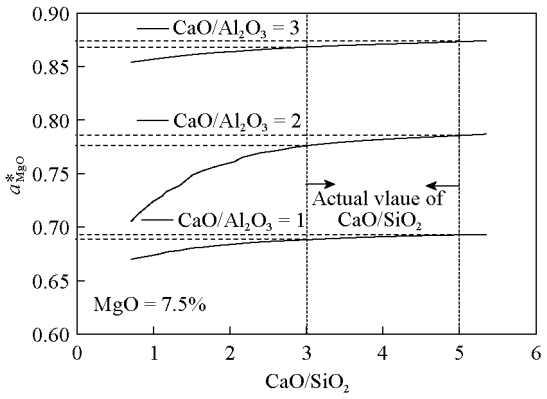

Fig. 12. Calculated relationship between the slag basicity and the activity of MgO in the slag (a^*_{MgO}).

4. Conclusions

(1) Typical Al_2O_3 and $Al_2O_3·SiO_2$ inclusions were observed in samples collected after Al was added and after silicomanganese was added, respectively. The $Al_2O_3·SiO_2$ inclusions started to transform into $MgO·Al_2O_3$ and $CaO–Al_2O_3–MgO$ inclusions in the tundish, which was similar to the observed behavior related to adhesion on the inner face of the submerged nozzle. Furthermore, the $CaO–Al_2O_3–MgO$ inclusions mostly transformed into $Al_2O_3·SiO_2·MgO$ in the examined slab samples.

(2) After the RH refining process, the MgO/Al_2O_3 mass ratio increased from 0.0005 to 0.3780. The percentage of $MgO·Al_2O_3$ spinel inclusions reached 58.4wt%, 59.0wt%, and 46.0wt% in samples collected after the RH refining process, from the tundish, and from the slab, respectively.

(3) The composition of the slag was similar to that of the inclusions, which indicated that slag entrapment was the source of the inclusions. The critical velocity of slag entrapment was calculated to be 0.45 $m·s^{-1}$ at 698 $L·min^{-1}$.

(4) When the test steel was in equilibrium with the slag, the [Mg] was 0.00025wt%, and the $[Al]_s$ was 0.32wt%, which was, according to our theoretical calculations, within the $MgO·Al_2O_3$ formation zone; consequently, $MgO·Al_2O_3$ inclusions formed in the steel.

(5) The formation of $MgO·Al_2O_3$ inclusions would be inhibited by reducing the quantity of the entrapped slag, controlling the roughing slag during casting, and controlling the slag composition and the MgO content in the ladle refractory.

References

[1] Y.Q. Song, J.S. Li, J. Li, Z.F. Wang, and S.F. Yang, $MgO·Al_2O_3$ based inclusions in gas cylinder steel during refining, *J. Univ. Sci. Technol. Beijing*, 31(2009), Suppl. 1, p. 130.

[2] J. Yang and X.H. Wang, Thermodynamics analysis and control of formation of magnesia–alumina spinel during refining of ultra-low oxygen, *Iron Steel*, 46(2011), No. 7, p. 26.

[3] K. Beskow, N.N. Tripathi, M. Nzotta, A. Sandberg, and S.C. Du, Impact of slag refractory lining reactions on the formation of inclusions in steel, *Ironmaking Steelmaking*, 31(2004), No. 6, p. 321.

[4] H. Itoh, M. Hino, and S. Banya, Thermodynamics on the formation of spinel nonmetallic inclusion in liquid steel, *Metall. Mater. Trans. B*, 28(1997), No. 5, p. 953.

[5] J.H. Park and D.S. Kim, Effect of $CaO–A1_2O_3–MgO$ slags on the formation of $MgO–A1_2O_3$ inclusions in ferritic stainless steel, *Metall. Mater. Trans. B*, 36(2005), No. 4, p. 495.

[6] J.H. Park, Formation mechanism of spinel-type inclusions in high-alloyed stainless steel melts, *Metall. Mater. Trans. B*, 38(2007), No. 4, p. 657.

[7] Y.J. Kang, F. Li, K. Morita, and S.C. Du, Mechanism study on the formation of liquid calcium aluminate inclusion from $MgO·Al_2O_3$ spinel, *Steel Res. Int.*, 77(2006), No. 1, p.785.

[8] C.W. Seo, S.H. Kim, S.K. Jo, M.O. Suk, and S.M. Byun, Modification and minimization of spinel ($Al_2O_3·x$MgO) inclusions formed in Ti-added steel melts, *Metall. Mater. Trans. B*, 41(2010), No. 4, p. 790.

[9] M. Jiang, X.H. Wang, B. Chen, and W.J. Wang, Laboratory study on evolution mechanisms of non-metallic inclusions in

high strength alloyed steel refined by high basicity slag, *ISIJ Int.*, 50(2010), No. 1, p. 95.

[10] M. Jiang, X.H. Wang, and W.J. Wang, Control of non-metallic inclusions by slag–metal reactions for high strength alloying steels, *Steel Res. Int.*, 81(2010), No. 9, p. 759.

[11] S.F. Yang, J.S. Li, Z.F. Wang, J. Li, and L. Lin, Modification of $MgO{\cdot}A1_2O_3$ spinel inclusions in Al-killed steel by Ca-treatment, *Int. J. Miner. Metall. Mater.*, 18(2011), No. 1, p. 18.

[12] Z.Y. Deng and M.Y. Zhu, Evolution mechanism of non-metallic inclusions in Al-killed alloyed steel during secondary refining process, *ISIJ Int.*, 53(2013), No. 3, p. 450.

[13] M. Jiang, B. Chen, W. Yang, and X.H. Wang, A study on thermodynamics of spinel inclusions formation in an alloy structural steel, *Spec. Steel*, 29(2008), No. 1, p. 16.

[14] M. Jiang, X.H. Wang, B. Chen, and W.J. Wang, Formation of $MgO{\cdot}Al_2O_3$ inclusions in high strength alloyed structural steel refined by $CaO–SiO_2–Al_2O_3–MgO$ slag, *ISIJ Int.*, 48(2008), No. 7, p. 885.

[15] H. Todoroki and K.Mizuno, Effect of silica in slag on inclusion compositions in 304 stainless steel deoxidized with aluminum, *ISIJ Int.*, 44(2004), No. 8, p.1350.

[16] J.H. Park and H. Todoroki, Control of $MgO{\cdot}Al_2O_3$ spinel inclusions in stainless steels, *ISIJ Int.*, 50(2010), No. 10, p. 1333.

[17] K. Fujii, T. Nagasaka, and M. Hino, Activities of the constituents in spinel solid solution and free energies of formation of MgO, $MgO{\cdot}Al_2O_3$, *ISIJ Int.*, 40(2000), No. 11, p. 1059.

[18] H. Lei, M.Y. Zhu, and J.C. He, Mathematical modeling of slag entrapment in continuous casting mould, *Acta Metall. Sin.*, 36(2000), No. 10, p. 1113.

[19] G. Okuyama, K. Yamaguchi, S. Takeuchi, and K. Sorimachi, Effect of slag composition on the kinetics of formation of Al_2O_3–MgO inclusions in aluminum killed ferritic stainless steel, *ISIJ Int.*, 40(2000), No. 2, p. 121.